AIP | The Journal of Chemical Physics

# Nitrogen dioxide fluorescence from N2O5 photolysis

Daniel Oh, Wade Sisk, Anthony Young, and Harold Johnston

Citation: The Journal of Chemical Physics **85**, 7146 (1986); doi: 10.1063/1.451348
View online: http://dx.doi.org/10.1063/1.451348
View Table of Contents: http://scitation.aip.org/content/aip/journal/jcp/85/12?ver=pdfcov

Published by the AIP Publishing

---

**Articles you may be interested in**

Laserinducedfluorescence study of the reaction of N2O with hot hydrogen atoms from 248 nm excimer laser photolysis of HIa)
J. Chem. Phys. **82**, 2295 (1985); 10.1063/1.448324

Photolysis of nitrogen dioxide
J. Chem. Phys. **59**, 4836 (1973); 10.1063/1.1680696

Kinetics of Nitrogen Dioxide Fluorescence
J. Chem. Phys. **51**, 1286 (1969); 10.1063/1.1672173

Fluorescence of Nitrogen Dioxide
J. Chem. Phys. **22**, 1693 (1954); 10.1063/1.1739877

The Entropies of Nitrogen Tetroxide and Nitrogen Dioxide. The Heat Capacity from 15°K to the Boiling Point. The Heat of Vaporization and Vapor Pressure. The Equilibria N2O4=2NO2=2NO+O2
J. Chem. Phys. **6**, 40 (1938); 10.1063/1.1750122

---

This article is copyrighted as indicated in the article. Reuse of AIP content is subject to the terms at: http://scitation.aip.org/termsconditions. Downloaded to IP: 128.62.36.173 On: Tue, 25 Nov 2014 22:22:42

# Nitrogen dioxide fluorescence from $N_2O_5$ photolysis

Daniel Oh, Wade Sisk, Anthony Young, and Harold Johnston
*Department of Chemistry, University of California and Materials and Molecular Research Division, Lawrence Berkeley Laboratory, Berkeley, California 94720*

(Received 27 May 1986; accepted 21 August 1986)

The products of ultraviolet photolysis of $N_2O_5$ are $NO_3$ and a wavelength dependent mixture of $NO_2$, $NO_2^*$, and NO + O, where $NO_2^*$ represents one or more excited electronic states of nitrogen dioxide. This $NO_2^*$ emits the visible fluorescence spectrum of nitrogen dioxide (photolysis induced fluorescence, PIF), and this spectrum was compared with monochromatically excited $NO_2$ fluorescence spectra (laser induced fluorescence, LIF). In a series of experiments, dispersed PIF and LIF spectra were measured where reactant pressure was 200 mTorr, delay time was 30 ns, and observation time was 600 ns. According to results obtained by Sugimoto and co-workers, under these conditions the continuous spectrum, which reflects the overall internal energy of $NO_2^*$, had been little modified by collision, although there was degradation of fine structure. The continuous LIF spectra were fit to an empirical function, and the PIF spectra were shown to be well represented by a linear combination of these mono-energetic excitation spectra. The coefficients of this linear combination plus other considerations were interpreted to give the almost nascent internal energy distribution of the electronically excited nitrogen dioxide molecules produced by $N_2O_5$ photolysis. This non-Boltzmann internal energy distribution indicates that electronically excited nitrogen dioxide is produced in the $^2B_1$ state when $N_2O_5$ is photolyzed.

## INTRODUCTION

Prior to direct observations of the products of $N_2O_5$ photolysis, it was presumed that the products would be one of three channels:

$$N_2O_5 + h\nu = NO_2 + NO_3 \quad (1)$$

$$= NO_2 + NO_2 + O \quad (2)$$

$$= NO_2 + NO + O_2. \quad (3)$$

Using a relatively slow (600 ns) flash-lamp pumped dye laser (doubled) to photolyze $N_2O_5$ and resonance fluorescence detection, Magnotta[1] obtained $0.3 \pm 0.1$ for atomic oxygen quantum yield between 290 and 300 nm. Photolyzing $N_2O_5$ with a fast (10 ns) excimer laser pulse and observing $NO_3$ with coaxial laser resonance absorption spectroscopy, Swanson *et al.*[2] directly observed the formation of $NO_3$ and obtained a quantum yield of $0.90 \pm 0.14$ at 248 nm. At low reactant pressure the quantum yield approached $1.0 \pm 0.1$. Using YAG laser photolysis at 266 nm and resonance fluorescence, Margitan[3] found an atomic oxygen quantum yield of $0.35 \pm 0.15$. At 290 nm, Barker *et al.*[4] found the quantum yield of $NO_3$ production to be $0.8 \pm 0.2$ and that for atomic oxygen production to be less than 0.1. Although these studies were not carried out at identical wavelengths, they appear to be contradictory in terms of channels (1 to 3). To resolve this apparent contradiction, Ravishankara *et al.*[5] photolyzed $N_2O_5$ at wavelengths between 248 and 355 nm, measuring both the atomic oxygen quantum yield and the quantum yield of $NO_3$. They found the quantum yield of $NO_3$ at 248 and 355 nm to be 0.96 (in agreement with Swanson *et al.*), and the quantum yield of atomic oxygen to be wavelength dependent: 0.72 at 248 nm, 0.38 at 266 nm (in agreement with Margitan), 0.21 at 287 nm, 0.15 at 289 nm, and zero above 307 nm. To explain these results Ravishankara proposed an additional channel for $N_2O_5$ photolysis

$$N_2O_5 + h\nu = NO_3 + NO + O. \quad (4)$$

According to Ravishankara, the photolysis of $N_2O_5$ occurs via channels (1) and (4), with a wavelength dependent partitioning between these two channels.

Whereas this mechanism resolves the apparent contradiction between the experimental studies, it raises an even more serious problem in terms of molecular dynamics. When the photo-excited $N_2O_5$ molecule falls apart partitioning its excess energy between translational energy and internal energy of the products, why does it systematically break the strong (72 kcal) N–O bond in $NO_2$ rather than the weak (49 kcal) N–O bond in $NO_3$? The structure of the $N_2O_5$ molecule is symmetrical about a central N–O–N linkage, and there is no structural feature that favors channel (4) over (2).[6] If an outer N–O bond broke to give atomic oxygen and unsymmetrical $N_2O_4$, the secondary products would be expected to be two molecules of $NO_2$ in view of the very fast reaction between $NO_3$ and NO to give the same products.[7] The idea that as the central N–O bond broke the triatomic $NO_2$ group would have a large excess of rovibrational energy over the four-atomic $NO_3$ group would constitute a major breakdown of statistical reaction rate theories, and this possibility should not be considered until other mechanisms are thoroughly examined. There are hints of another mechanism in the literature. Nelson *et al.*[8] detected $NO_2$ fluorescence following $N_2O_5$ photolysis, but did not pursue the phenomenon. Upon photolysis, $N_2O_4$ is known[9] to give $NO_2$ fluorescence, and photolysis of nitromethane gives $NO_2$ fluorescence.[10] These studies suggest that as a central N–O bond of photoexcited $N_2O_5$ breaks, the excess energy is par-

0021-9606/86/247146-13$02.10 © 1986 American Institute of Physics

This article is copyrighted as indicated in the article. Reuse of AIP content is subject to the terms at: http://scitation.aip.org/termsconditions. Downloaded to IP: 128.62.36.173 On: Tue, 25 Nov 2014 22:22:42

titioned between $NO_3$ and electronically excited nitrogen dioxide, $NO_2^*$:

$$N_2O_5 + h\nu = NO_3(v,J) + NO_2^*(v,J) + E(trans). \quad (5)$$

As the electronic energy internally converts to internal excitation, the bond breaks if the total internal energy exceeds the bond energy. If the sum of electronic, vibrational, and rotational internal energy does not exceed the bond energy, the excited molecule exists as a linear combination of electronically excited ($^2B_2$ and $^2B_1$) states plus highly vibrationally excited ground electronic state ($^2A_1$), the "Douglas effect".[11] Such a state eventually fluoresces or it is deactivated by collision.[12,13]

At sufficiently low pressures and for sufficiently early times of observation the $N_2O_5$ photolysis induced fluorescence (PIF) of nitrogen dioxide should give information about the "nascent" internal energy distribution of the $NO_2^*$ product, if one had a sufficiently detailed set of laser induced fluorescence (LIF) spectra of $NO_2$ to act as a "basis set" for the PIF spectra. This article involves an attempt to carry out this method of interpreting PIF data, and it includes new PIF and LIF data. Although recent studies of nitrogen dioxide fluorescence have emphasized high resolution spectral features,[14] this investigation gets its information about the broad aspects of the internal energy distribution of the photolysis product from the shape of the continuum spectrum of $NO_2$ fluorescence.

During the course of this study, it was found that other molecules, $ClNO_2$ and $HNO_3$, give visible $NO_2$ fluorescence upon ultraviolet photolysis, and further work is underway on these molecules.

## EXPERIMENTAL

The experimental arrangement is shown in the schematic diagram, Fig. 1. The photolysis source was a Quanta-Ray DCL-II Nd:YAG pumped dye laser (PDL-I) output, which was frequency doubled through an Inrad doubling crystal/auto tracking unit. This system was obtained on loan from the San Francisco Laser Center. The pulse duration was 9 ns, and the pulse energy width was 1.0 $cm^{-1}$ for second, third, and fourth harmonic output and 0.5 $cm^{-1}$ for the dye laser output. The UV laser output was separated from the visible output by a Pellin Brocca prism, and was further collimated with an iris in front of the photolysis cell. The collimated beam was about 4 mm in diameter, and was guided through three more apertures before the Scientech power meter. These apertures were kept in place throughout the experiment in order to reproduce the beam path and the beam size.

The reactant gas flowed through the photolysis cell, and its concentration was monitored by the pressure measured with MKS Baratron Model 220-2A6-100 capacitance manometer and by UV absorption spectroscopy. The UV absorption monitoring system consisted of a deuterium lamp, whose output was chopped at 400 Hz, collimated by a 10 cm focal length quartz lens, propagated through a Pyrex absorption cell (2.3 cm diameter, 100 cm length) equipped with Suprasil windows, dispersed by a Bausch & Lomb Model ND 45 monochromator with a 2700 lines/mm grating blazed at 200 nm, and focused on an RCA 1P28 photomultiplier tube. The signal from the PMT was amplified and sent to a home-built lock-in amplifier.

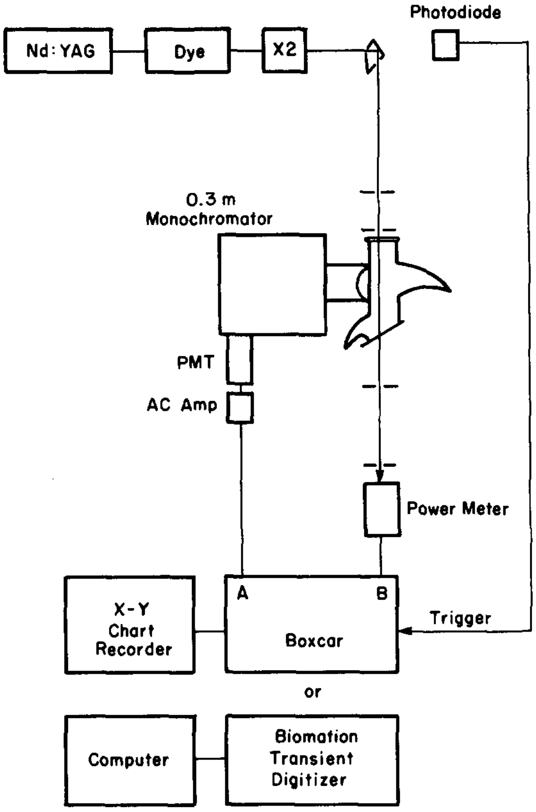

FIG. 1. Schematic diagram of the experimental apparatus.

The fluorescence signal was collected with an $f/1.5$ lens, and was focused on the slit of a 0.3 m McPherson monochromator (model 218) which had a 1200 lines/mm grating blazed at 5000 Å. For the total fluorescence intensity measurement, the grating was positioned at the zeroth order reflection angle while the slits were opened to the maximum width (2 mm). For the dispersion of the fluorescence, the slits were typically set at 500 $\mu$m resulting in a full width at half maximum of about 3 mm.

The fluorescence was detected at the exit of the monochromator with an RCA C31034 photomultiplier. It has a flat, highly sensitive response from 300 to 850 nm. The signal from the PMT was terminated with a 50 ohm resistor for fast response, and was amplified with an Avantech three-stage AC amplifier (model GPD 461, 462, and 463). This home-assembled amplifier had a fairly flat 35 dB gain from 100 Hz to 160 MHz.

The signal from the amplifier was processed by an SRS gated integrator/boxcar averager for either the total fluorescence measurement or the dispersed emission spectrum. Typically, the boxcar gates had a 0–38 ns delay and a 600 ns width. These signal processors were triggered by pulses coming from a photodiode detector observing the scattered laser output.

The laser energy was monitored with a Scientech power meter (model 360001), which had been calibrated against a factory calibrated power meter. Output from the Scientech was fed to a second gated integrator/boxcar averager and was DC coupled for the voltage measurement.

This article is copyrighted as indicated in the article. Reuse of AIP content is subject to the terms at: http://scitation.aip.org/termsconditions. Downloaded to IP: 128.62.36.173 On: Tue, 25 Nov 2014 22:22:42

The $N_2O_5$ was prepared by the method of Schott and Davidson.[15] The $O_2$ was passed through a heated copper tube and a $P_2O_5$ drying column to remove moisture and hydrocarbon impurities before it entered the ozonizer (Ozone Research & Equipment Corporation). A small portion of purified $O_2$ was bubbled through a Pyrex bubbler containing $NO_2$, and the $NO_2$ was reacted with the $O_3$ from the ozonizer at the *T*-joint. The $N_2O_5$ was collected in a trap held at $-77$ C with an isopropanol/dry ice slush bath. Each batch of $N_2O_5$ was pumped on while held in $CCl_4$ slush bath ($-29$ C) before each experiment. The purity of the sample was checked by monitoring the UV absorption profile[16] while a known pressure of sample was flowing. The main impurity was thought to be $HNO_3$ formed from the reaction between $N_2O_5$ and the residual moisture on the wall of the trap. There appeared to be about 10%-15% $HNO_3$ in the $N_2O_5$ sample, but no further attempts were made to purify the sample since the photolysis wavelengths were in the range where $N_2O_5$ absorption cross sections were large compared to that of $HNO_3$. $NO_2$ was not a detectable impurity since it reacted in the presence of excess $O_3$.

The $NO_2$, used for the LIF experiments, was taken out of the tank. Then, the freeze–pump–thaw procedure was performed in order to remove mainly NO impurities. The purified $NO_2$ was stored in a darkened Pyrex bulb until ready to use.

The wavelengths used for $N_2O_5$ photolysis and for $NO_2$ laser induced fluorescence are given in Table I, including the configuration of the YAG laser and the dye used.

## RESULTS

There were two main types of results in this study: (i) Laser induced fluorescence (LIF) of nitrogen dioxide excited by a pulse of radiation of about 10 ns duration and at wavelengths between 460 and 640 nm. (ii) Photolysis induced fluorescence (PIF), that is, fluorescence of $NO_2$ in the visible spectral region by pulsed photolysis of nitrogen pentoxide in the ultraviolet region at wavelengths between 266 and 304.5 nm. For each of these two types of study, two kinds of experimental data were taken: (a) The fluorescence was dispersed through a 0.3 m monochromator and sampled for 600 ns after a 30 ns delay time. (b) The monochromator was set to zero order and total fluorescence was observed after a delay of 30 ns and for a sampling period of 600 ns.

The raw data of the dispersed $NO_2$ LIF excited at 460, 532, 560, 584 (duplicate runs), and 640 nm are shown in Figs. 2 and 3. The total pressure was 200 mTorr, and the data were taken during the first 600 ns after a 30 ns delay time, which included the 10 ns time width of the photolysis beam. In all cases there was a broad fluorescence band, which originated at energies about 600 $cm^{-1}$ above the exciting light and extends across the rest of the visible spectrum. There are some variations above the continuous background. Some variations are real, reproducible structure, and some are experimental noise as can be seen by comparison of duplicate runs, which were taken in every case. One pair of duplicate runs is shown in Fig. 3 for data excited at 584 nm, and it can be seen that many of the features are duplicated. In the spectrum taken at 640 nm, the tall sharp spikes are reproducible spectral features, but most of the variation is noise. At this wavelength the $NO_2$ optical absorption cross section is very small, and the data are especially noisy. At 532 nm the spectral features are much stronger than those at 460 or 560 nm. The points circled in Figs. 2 and 3 are calculated, as discussed in a later section. The short-time narrow-band LIF of $NO_2$ is known to be very complicated[12–14,17] with sharp spectral features rising out of the broad continuous background. The object of this investigation is not to study the spectral fine structure, but rather to characterize the initial broad continuous fluorescence and to use this information to analyze the energy distribution of $NO_2$ produced by photolysis of $N_2O_5$.

One example of dispersed photolysis induced fluorescence (PIF) is shown in Fig. 4, where $NO_2$ visible fluorescence produced by $N_2O_5$ photolysis is presented. The pressure of $N_2O_5$ was 200 mTorr, the temporal observation window was 600 ns, and the photolysis wavelength was 266 nm. The fluorescence spectrum is a broad feature stretching from about 420 to 800 nm. In particular, this spectrum is broader than any of the monochromatically excited LIF spectra. The "structure" shown by this spectrum is almost entirely noise. In the upper left-hand corner of Fig. 4, there are three duplicate sweeps between 350 and 500 nm with much larger number of shots averaged per unit wavelength than was used for the full spectrum. These data were taken to characterize the wavelength threshold of the PIF. Data analogous to these were taken also at 280, 292, and 304.5 nm.

The quantum yield for $NO_2$ fluorescence upon $N_2O_5$ photolysis can be estimated by comparing the fluorescence

TABLE I. Wavelengths used for $N_2O_5$ photolysis and for $NO_2$ laser induced fluorescence.

| Type | Wavelength/nm | YAG configuration | Dye used | Doubled |
|---|---|---|---|---|
| PIF | 266 | 4th harmonic | None | No |
| | 280 | 2nd harmonic | R6G | Yes |
| | 292 | 2nd harmonic | Kiton red | Yes |
| | 304.5 | 2nd harmonic | SR 640 | Yes |
| LIF | 460 | 3rd harmonic | Coumarine 460 | No |
| | 532 | 2nd harmonic | None | No |
| | 560 | 2nd harmonic | R6G | No |
| | 584 | 2nd harmonic | Kiton red | No |
| | 640 | 2nd harmonic | DCM | No |

This article is copyrighted as indicated in the article. Reuse of AIP content is subject to the terms at: http://scitation.aip.org/termsconditions. Downloaded to IP: 128.62.36.173 On: Tue, 25 Nov 2014 22:22:42

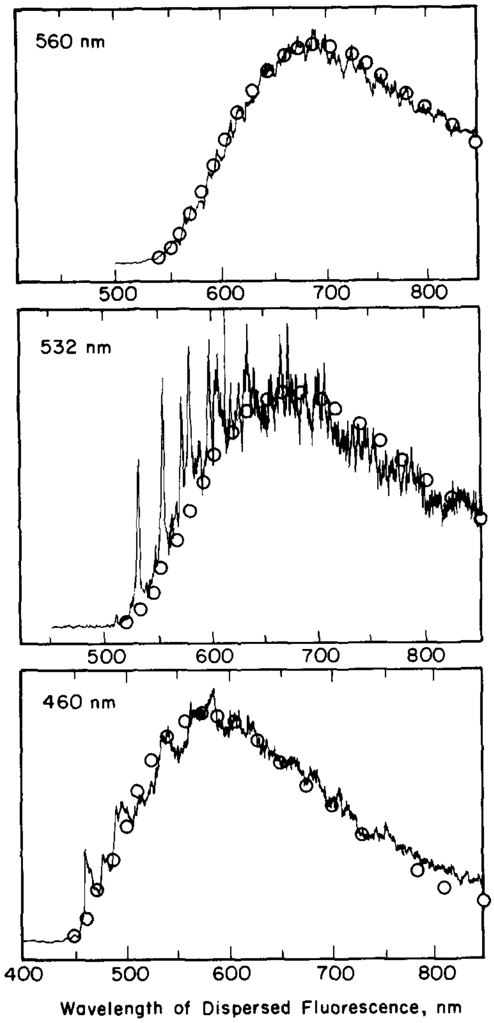

FIG. 2. Raw experimental data for the laser induced fluorescence of nitrogen dioxide where the pressure of $NO_2$ is 200 mTorr, the delay time between laser pulse and start of observations was 30 ns, and the window of observation was 600 ns. Running average fluorescence spectra were recorded as the 0.3 m monochromator was slowly scanned. The circled points were calculated according to the empirical fitting function, Eqs. (6) and (9), for which the only difference between one curve and another is the wavelength of the excitation. Under these conditions there is calculated to be about one hard spheres collision between laser excitation and the end of the observation period. However, it is known that there is substantial rotational energy redistribution and some vibrational energy loss under these conditions (Refs. 12–14, 17).

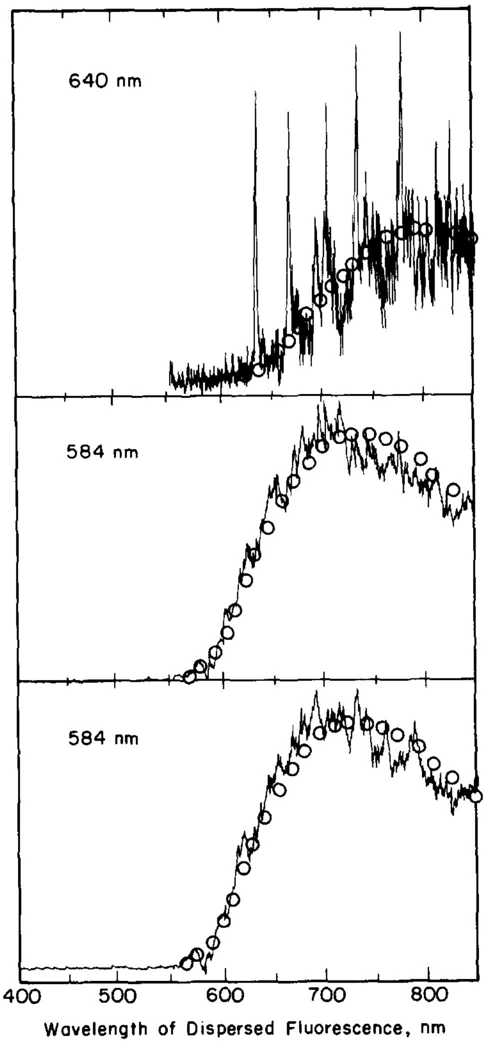

FIG. 3. Same as Fig. 2 with different excitation wavelengths.

intensity in arbitrary units between LIF and PIF experiments. Corrections had to be made for different amplifier settings, optical absorption cross sections, and laser energy. Table II presents the intensity of total fluorescence when $NO_2$ is excited at various visible wavelengths; the units are volts of signal times $10^{13}$ divided by photons absorbed $cm^{-3}$ with a delay of 30 ns after the laser flash and for a duration of 600 ns. Table III gives similar results when $NO_2$ fluorescence was caused by $N_2O_5$ photolysis.

## DISCUSSION

The goal of this experiment was to detect the "nascent" internal energy distribution of $NO_2^*$ as it was produced from $N_2O_5$ photolysis. The first question to consider is how many collisions the product molecules underwent up to the completion of the observation period, 600 ns. With nitrogen dioxide excitation at 463 nm, Sugimoto *et al.*[13] observed fluorescence as a function of wavelength (475–720 nm), pressure (1–150 mTorr), and at times from 130 to 4000 ns. With $NO_2$ as energy transfer gas, they obtained three different quenching rate constants (in multiples of $10^{-10}$ $cm^3\ s^{-1}$): 16 for quenching high resolution rotational features, 5.3 for quenching high resolution vibrational features, and 1.1 for quenching total energy of the excited electronic state. At the standard experimental conditions used in the present study, 200 mTorr and 600 ns observation period, there would be 6.3 collisions degrading the rotational distribution, 2.1 collisions degrading the vibrational distribution, and about 0.4 collisions removing total energy from the excited electronic manifold in the LIF experiments. On the basis of experiments done here with $N_2O_5$ and with $NO_2$ as energy transfer gases (unpublished data), these numbers of collisions should be approximately doubled in the PIF experiments, where $N_2O_5$ is the energy transfer gas. Sugimoto *et al.*[13] showed one figure where the $NO_2$ pressure was 150 mTorr and the observation period extended from 130 to 4000 ns. Between 130 and 1000 ns their dispersed fluorescence spectrum showed a detectable degradation of structured fea-

This article is copyrighted as indicated in the article. Reuse of AIP content is subject to the terms at: http://scitation.aip.org/termsconditions. Downloaded to IP: 128.62.36.173 On: Tue, 25 Nov 2014 22:22:42

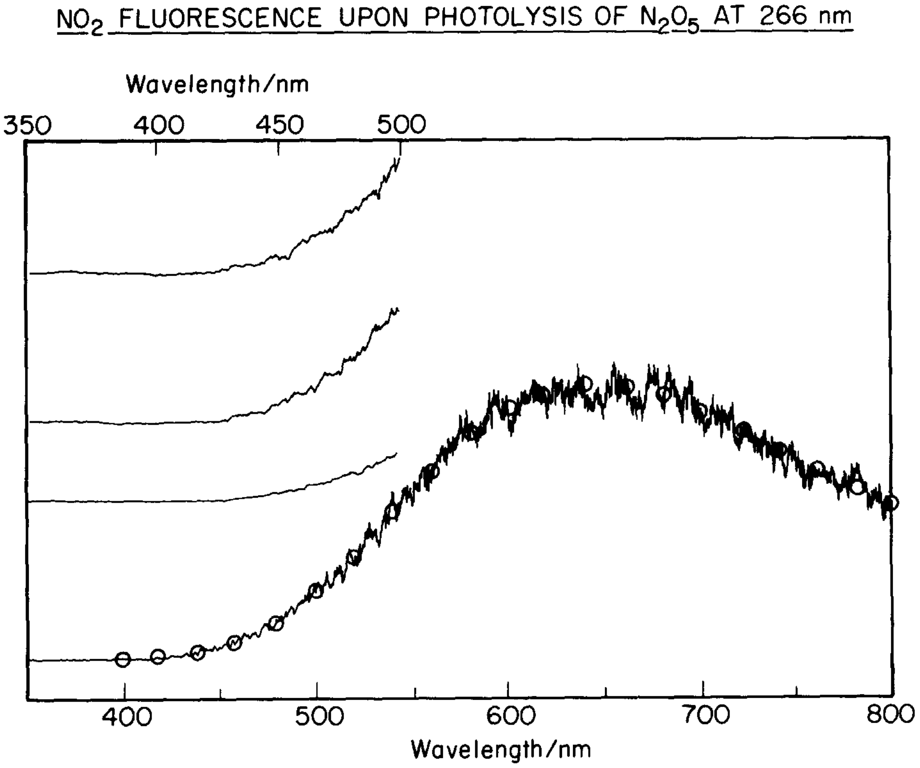

FIG. 4. Raw experimental data for the fluorescence of nitrogen dioxide upon ultraviolet (266 nm) photolysis of $N_2O_5$ where the pressure of $N_2O_5$ was 200 mTorr, observation delay time was 30 ns, and window of observation was 600 ns (the same as that for Figs. 2 and 3). The inset figures at the upper left-hand side of the figure were slow-scan repeat runs over the threshold region, involving longer averaging times than the complete wavelength scan and different amplifier settings. A smooth curve was drawn through the spectrum, which is given at regular wavelength intervals by the circles shown on the figure.

tures, but there was no noticeable alteration of the overall envelope of the spectrum. It is concluded that in the experiments reported here, collisions modified somewhat the true nascent distribution of internal energy states of the electronically excited product molecules and modified the distribution of the laser induced $NO_2$ fluorescence, but these modifications were small enough that this study detected fluorescence from very nearly the nascent energy distribution of the product molecules.

The PIF spectrum observed here came from $NO_2$, and no contribution from $NO_3$ fluorescence[8] could be detected. The origin of the PIF spectrum was 400 nm, the same as that for $NO_2$. The origin of the $NO_3$ fluorescence spectrum is 580 nm. None of the PIF spectra showed enhancement at 662 nm, where the $NO_3$ spectrum shows its strongest feature.

PIF data were observed with $N_2O_5$ photolysis at 266, 280, 292, and 304.5 nm. In each case a smooth curve was drawn through the experimental PIF data, and special emphasis was given to the threshold region illustrated by the three curves inset in Fig. 4. Points were selected every 20 nm between 400 and 800 nm (compare the circles in Fig. 4). These curves were normalized by the maximum intensity to give relative PIF intensity as a function of fluorescence wavelength. Such curves for photolysis at 266 and 304.5 nm are shown in Fig. 5.

By simple inspection of the data, two interpretations of the PIF spectra can be given. In Fig. 5 the distribution of PIF lies at higher energy (shorter wavelength) when photolysis occurred at the higher energy (266 vs 304.5 nm), giving the nonsurprising interpretation that the higher the energy of photolysis the higher the energy of the product $NO_2^*$ molecule. The PIF curve at 266 nm is compared with two LIF curves taken at 460 and 532 nm in Fig. 6, and it can be seen that the energy spread in the PIF curve is broader than the mono-energetically excited LIF curves. The threshold of the PIF curve is slightly on the blue side of the 460 nm LIF curve, and the long-wavelength portion of the PIF curve is close to that of the 532 nm LIF curve. A single LIF curve corresponds to a delta function of excitation energy, but this narrow excitation energy projects to the excited state the Boltzmann distribution of rotational–vibrational energy of the room temperature nitrogen dioxide molecule. Figure 6 shows that the internal energy distribution of photolysis pro-

TABLE II. Total undispersed $NO_2$ fluorescence when excited by YAG-dye laser at various wavelengths (nm) and for various pressures (mTorr) of pure $NO_2$. The units are arbitrary (volts of signal at fixed amplification factors per $10^{13}$ photons absorbed by $NO_2$). The signal was collected in a boxcar integrator with 30 ns delay time after laser flash and with 600 ns observation window. The grating in the monochromator was set at zero order to collect all wavelengths of fluorescence.

| nm | mTorr | 20 | 40 | 60 | 90 |
|---|---|---|---|---|---|
| 640 | | 130 | 107 | 96 | 64 |
| 609 | | 103 | 81 | 63 | 63 |
| 585 | | 139 | 151 | 131 | 113 |
| | Average | 124 | 113 | 97 | 80 |

TABLE III. Same as Table II, except the reactant is pure $N_2O_5$ and the observations are of undispersed $NO_2$ emission.

| nm | mTorr | 20 | 40 | 60 | 100 | 150 | 200 |
|---|---|---|---|---|---|---|---|
| 266 | | 28 | 24 | 23 | 20 | 17 | 16 |
| 280 | | 28 | 26 | 28 | 16 | 11 | 10 |
| 292 | | 26 | 26 | 10 | 17 | 13 | 9 |
| 304.5 | | 3.3 | 2.8 | 2.7 | 2.0 | 1.5 | 1.2 |
| 320 | | 3.0 | 3.2 | 2.7 | 2.2 | 2.1 | 1.5 |

This article is copyrighted as indicated in the article. Reuse of AIP content is subject to the terms at: http://scitation.aip.org/termsconditions. Downloaded to IP: 128.62.36.173 On: Tue, 25 Nov 2014 22:22:42

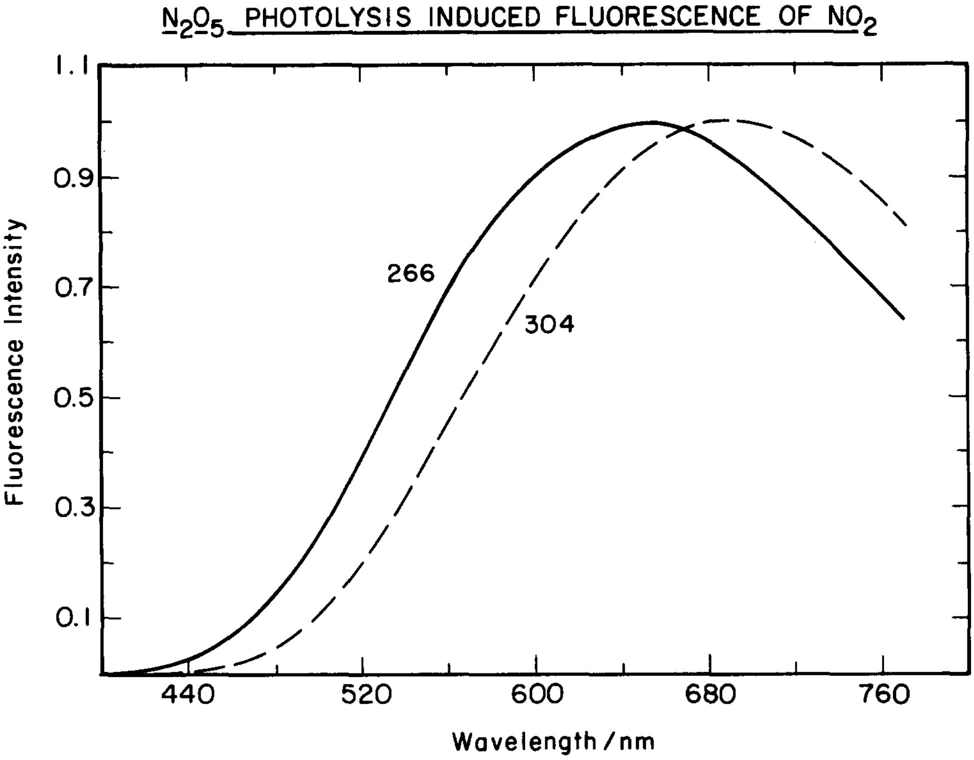

FIG. 5. Smoothed relative dispersed $NO_2$ fluorescence spectra following photolysis of $N_2O_5$ at two different wavelengths. The red shift of the observed spectrum excited at the longer ultraviolet wavelength qualitatively implies a lower and different internal energy distribution.

duced $NO_2^*$ is broader than that of ground-state room temperature $NO_2$. By use of the LIF observed data (Figs. 2 and 3), these obvious qualitative interpretations of Figs. 5 and 6 are turned into an estimate of the excited $NO_2$ internal energy distribution in the PIF experiments in the paragraphs below.

A simple empirical expression was found for the average observed LIF curves, Figs. 2 and 3:

$$L(X,Y) = AZ^2 \exp(1-Z^2), \tag{6}$$

$$Z = [(Y-X)/(Y-X_M)], \tag{7}$$

where $X$ is the fluorescence energy in $cm^{-1}$, $Y$ is the threshold energy of the fluorescence spectrum, $X_M$ is the energy at the fluorescence maximum intensity, $A$ is the amplitude at the maximum intensity, $Z$ is the quantity defined by Eq. (7), and $L(X,Y)$ is the fluorescence intensity dispersed over $X$ and with origin at $Y$. Furthermore, it was found that as an average

$$Y/X_M = 1.31. \tag{8}$$

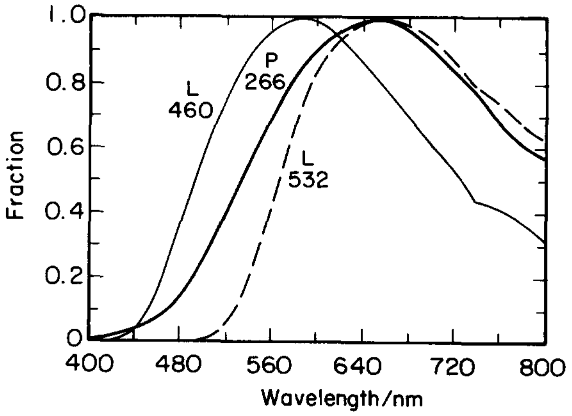

FIG. 6. Comparison of nitrogen dioxide LIF at 460 and at 532 nm with the nitrogen dioxide luminescence produced from $N_2O_5$ photolysis at 266 nm. This figure directly shows that the PIF spectrum is broader in energy than the mono-energetically excited LIF spectra.

With this empirical value the term $Z$ is simply

$$Z = [(Y-X)/(0.235\,Y)]. \tag{9}$$

For each fluorescence curve normalized to maximum intensity, the only adjustable parameter is the threshold frequency $Y$, but even this can be estimated by adding 600 $cm^{-1}$ to the laser excitation frequency. The circles shown in all the curves of Figs. 2 and 3 were calculated according to the above expressions. In the continuum, the average relative fluorescence intensity at all wavelengths of LIF is well given by Eqs. (6) and (9).

The empirical LIF spectra are normalized to unit area under the curves by dividing Eq. (6) by

$$\begin{aligned} L &= -\int_{25\,000}^{0} L(X,Y)dX \\ &= -Ae(Y-X_M)\int_0^{Y/(Y-X_M)} Z^2\exp(-Z^2)dZ. \end{aligned} \tag{10}$$

Using Eq. (9), one sees that the upper limit in the integral is 1/0.235 or 4.255. When $Z$ is equal to 4.255, the value of $Z^2\exp(-Z^2)$ is $2.5\times10^{-7}$, so that the upper limit of the integral is effectively infinity. With this upper limit, Eq. (10) is a standard definite integral of value $\sqrt{\pi}/4$. To this approximation, the value of $L$ is $0.104\,13\,AeY$. The normalized LIF spectra are

$$L_D dX = L(X,Y)dX/L = (9.603/Y)Z^2\exp(-Z^2)dX. \tag{11}$$

$P(X)$ is defined as the normalized intensity of a PIF curve, such as those illustrated by Fig. 5, after conversion from wavelength to photon energy units. A systematic pro-

This article is copyrighted as indicated in the article. Reuse of AIP content is subject to the terms at: http://scitation.aip.org/termsconditions. Downloaded to IP: 128.62.36.173 On: Tue, 25 Nov 2014 22:22:42

cedure was worked out to fit the $P(X)$ curves with a linear superposition of LIF curves:

$$P(X) = -\int_{25\,000}^{X} L_D(X,Y)F(Y)dY, \tag{12}$$

where $F(Y)$ is the fraction of a LIF curve [Eq. (11)] excited with a threshold energy of $Y$. The first method used is illustrated with the aid of Fig. 7, where the PIF threshold energy (LIF energy plus 600 $\text{cm}^{-1}$) is the $Y$ axis and a finite set of LIF spectra generated by 7 values of $Y$ are along the $X$ axis. For some energy $X_i$ of the PIF dispersed spectrum, its components are, in this simplified case, the sum of the weighted LIF curves arising to the left

$$P(X_i) = \sum_{j=0}^{i-1} L_D(X_i,Y_j)F(Y_j)\Delta Y_j, \tag{13}$$

where $F(Y_j)$ is the weighting factor. To obtain the weighting factors, one starts with a point on the PIF curve close to the threshold. With the grid shown in Fig. 4, the first nonzero value is at 440 nm, and this would be taken as $X_1$. With the grid illustrated by Fig. 7, the PIF spectra at energy $X_1$ has only one term contributing to it, and the first term of $F$ can be evaluated directly from the data

$$F_1 = P(X_1)\text{obs}/[L_D(X_1,Y_0)\Delta Y_0]. \tag{14}$$

At all values of $X$, the contribution of the first term in Eq. (13) is $F_1 L_D(X,Y_0)\Delta Y_0$, and this is subtracted from the observed PIF spectrum. The residue has a unique value of $F$ arising from $Y_1$. The operation is repeated on the next higher panel of the triangular structure of Fig. 7, and it is repeated term by term until the full PIF spectrum is accurately reproduced by the weighted LIF spectra.

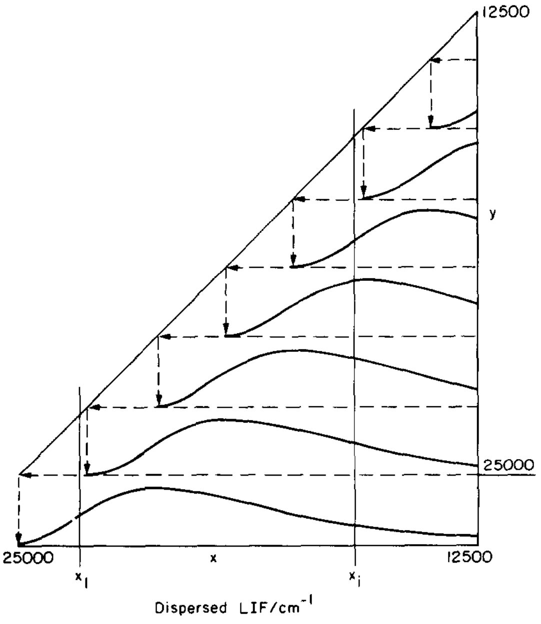

FIG. 7. A simplified diagram showing how the observed PIF spectrum (at $X_i$ in this example) may be regarded as a linear superposition of LIF spectra that have excitation energies to the left of $X_i$ and are independent of LIF spectra with excitation energies to the right of $X_i$. Also, this diagram when referred to $X_1$ shows how the weighting factors $F(Y_j)$ may be evaluated one term at a time.

This procedure was carried out with a set of 21 equally spaced wavelengths between 400 to 800 nm, which were converted to energy (wave number) units and used in Eq. (13). Starting at the highest observed energy of PIF, the coefficients $F(Y)$ are evaluated one at a time. The first set of coefficients found in this way was smoothed, and the procedure was repeated. An example of this procedure is given by the step function in Fig. 8, and the 11 values of $F(Y)$ found in this way give a good representation of the observed PIF spectrum. However, when this step function was summed and plotted on probability paper, it was seen to be a Gaussian function, which is also given in Fig. 8:

$$F(Y) = \exp[-(Y-\mu)^2/2\sigma^2]/(2\pi\sigma^2)^{1/2}. \tag{15}$$

The step functions of $F(Y)$ found from the PIF spectra at 280, 292, and 304.5 nm also gave good Gaussian functions. From a set of noisy experimental data, it is much easier to fit the two parameters of the Gaussian function ($\mu$, mean; $\sigma$, standard deviation) than the ten or so individual values of $F$.

For the second method of evaluating the weighting function $F(X)$, it is assumed to be a Gaussian function. The observed PIF spectrum $P(X)$ was represented by the integral

$$P(X) = -\frac{9.603B}{(2\pi\sigma^2)^{1/2}}\int_{25\,000}^{X} \exp\left[-\frac{(Y-\mu)^2}{2\sigma^2}\right]\left(\frac{Y-X}{aY}\right)^2 \times \exp\left[-\left(\frac{Y-X}{aY}\right)^2\right]\frac{dY}{Y}, \tag{16}$$

where $B$ is the amplitude factor and $a = 0.235$. The energy range 25 000 to 12 500 was divided into 125 equally spaced intervals, and the integral (16) was evaluated as a sum over this energy grid. For each PIF curve, values of $\mu$ and $\sigma$ were estimated and used in Eq. (16), and these quantities were varied until the calculated (16) curve agreed with the experimental spectrum. The inferred threshold energy distributions and a comparison between observed and calculated PIF spectra are given by Figs. 8–11. The method is sensitive to about 100 $\text{cm}^{-1}$ both in the value of $\mu$ and $\sigma$. The fitted values of $\mu$ and $\sigma$ are given in Table IV for each of four wavelengths of $N_2O_5$ photolysis. At high photolysis energies, the standard deviation of the distribution of threshold energies is somewhat larger than it is at low photolysis energies.

The curves $F(Y)$ give the distribution of threshold energies that reproduce the PIF spectrum; they do not give the population of excited molecules produced by photolysis. To get an estimate of this populations, two additional factors must be considered: (1) Each mono-energetic excitation energy projects into the excited state the ground-state rotational–vibrational energy distribution and (2) the lifetime of electronically excited nitrogen dioxide varies with excitation energy.

Using the method of Pitts, Sharp, and Chan,[18] the rotational–vibrational energy of nitrogen dioxide at 300 K was calculated, including rotational quantum number $K$ from 1 to 12. The superposition of the various rotational $K$ curves confers some irregularity to the distribution function, which is given for a number of energies as circles on Fig. 12. The excited vibrational states give a very small contribution above 800 $\text{cm}^{-1}$, but the curve in Fig. 12 is almost entirely

This article is copyrighted as indicated in the article. Reuse of AIP content is subject to the terms at: http://scitation.aip.org/termsconditions. Downloaded to IP: 128.62.36.173 On: Tue, 25 Nov 2014 22:22:42

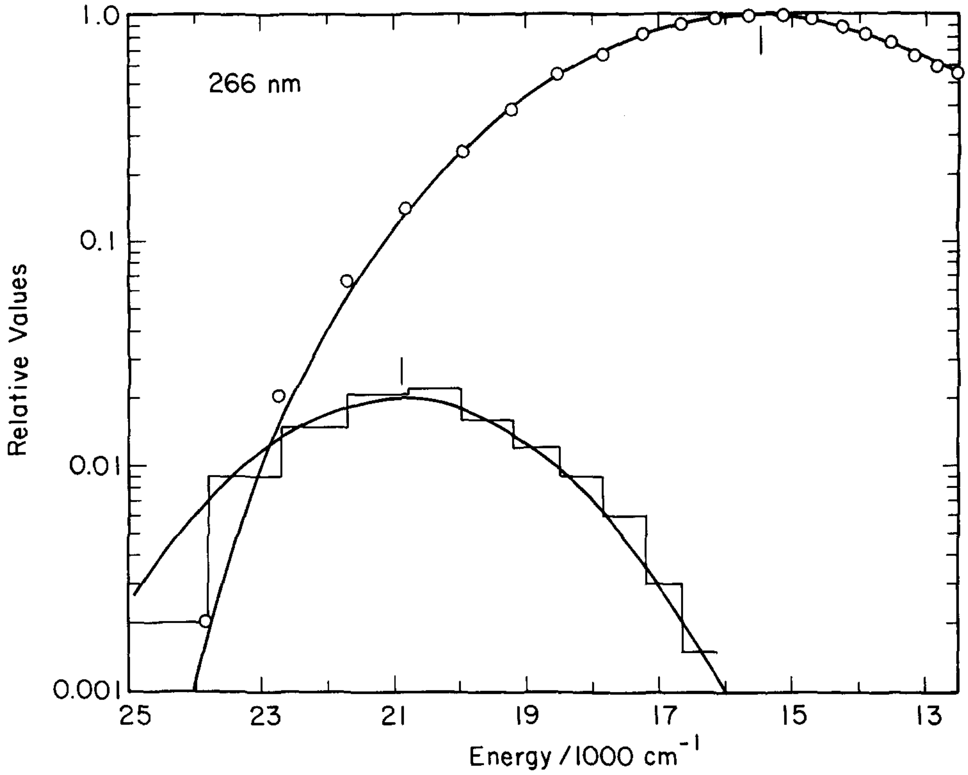

FIG. 8. Observed relative $NO_2$ fluorescence (PIF) as function of wavenumber following photolysis of $N_2O_5$ at 266 nm, circles. Weighting factors $F(X_i)$ based on term by term solution of triangular matrix as indicated by Fig. 7 and Eqs. (13) and (14), step function. The smooth curve through the step function is a Gaussian function (15). The smooth curve through the experimental points is the calculated PIF spectrum based on the Gaussian function and Eq. (16).

the room temperature rotational energy distribution. The smooth curve in Fig. 12 is

$$D(E) = C(E/kT)\exp[1 - (E/kT)], \qquad (17)$$

where $C$ is the maximum amplitude, $E$ is energy in cm$^{-1}$, and $kT$ is 208 cm$^{-1}$. The experiments were carried out at about 293 K, and $kT$ was taken to be 200 cm$^{-1}$ in applying Eq. (17) to this problem.

Donnelly and Kaufman[12] measured the radiative lifetime of nitrogen dioxide as a function of laser excitation wavelength, which they extrapolated to zero pressure. The excitation energies covered the range 15 000–22 000 cm$^{-1}$, and they gave an empirical function that covered this range. By extrapolation beyond their range of observations, values of fluorescence lifetime were obtained between 12 500 and 25 000 cm$^{-1}$, as listed in Table V. To correspond to thresh-

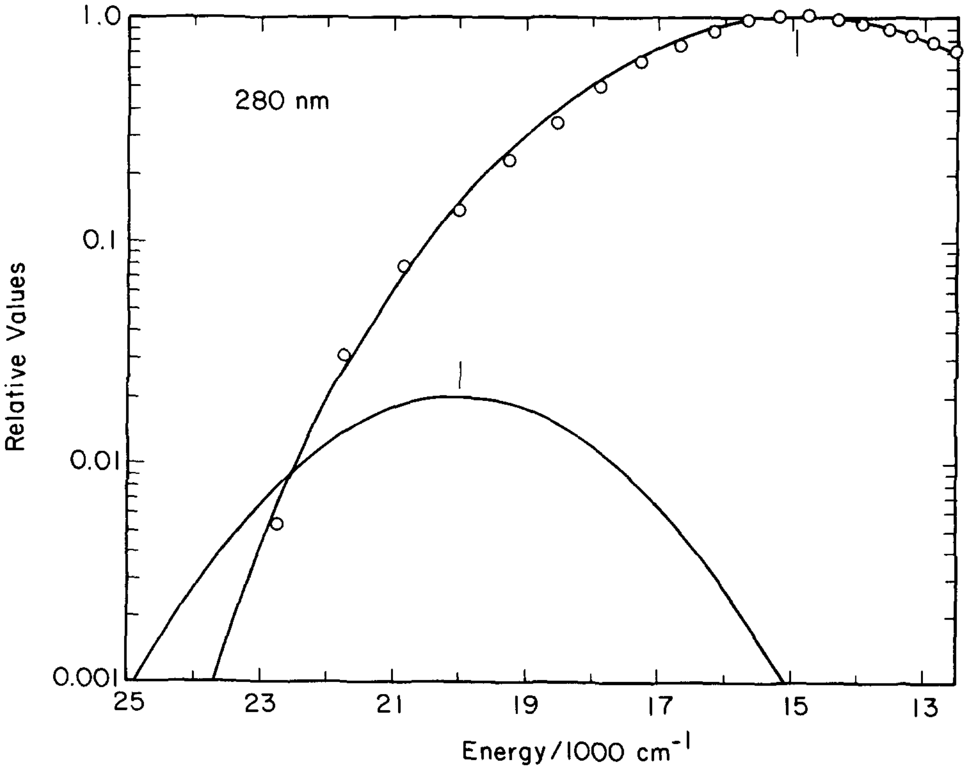

FIG. 9. Same as Fig. 8, except for omission of step function; photolysis occurred at 280 nm.

This article is copyrighted as indicated in the article. Reuse of AIP content is subject to the terms at: http://scitation.aip.org/termsconditions. Downloaded to IP: 128.62.36.173 On: Tue, 25 Nov 2014 22:22:42

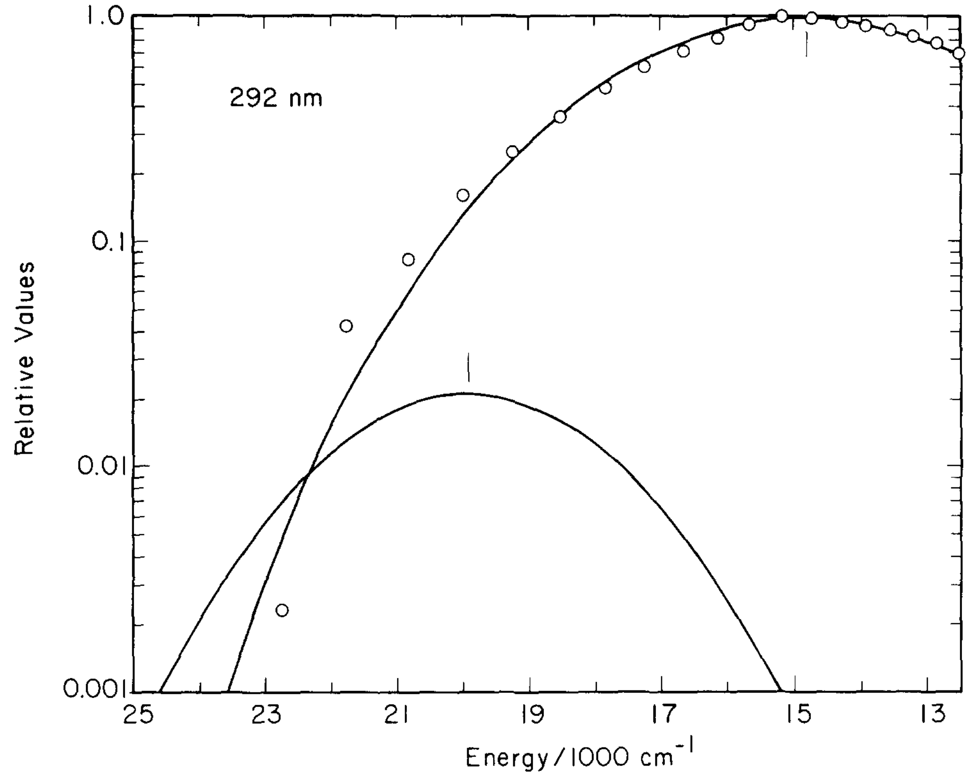

FIG. 10. Same as Fig. 9; photolysis occurred at 292 nm.

old energies $Y$, 600 cm$^{-1}$ is added to the laser excitation energies. The ratio of lifetime at any threshold energy to that at 25 000 cm$^{-1}$ is defined as $T(E)$. For a given fluorescence intensity, the population is directly proportional to the lifetime.

From these considerations, the population of the photolysis produced excited nitrogen dioxide molecules as a function of energy $E$ is given by

$$\begin{aligned}\mathrm{POP}(E) &= -\int_{25\,000}^{E} F(Y)T(Y)D(Y-E)dY \\ &= -A\int_{25\,000}^{E} \frac{\exp[-(Y-\mu)^2/2\sigma^2]}{(2\pi\sigma^2)^{1/2}} \\ &\quad \times T(Y)\left\{\frac{Y-E}{200}\exp\left[-\frac{(Y-E)}{200}\right]\right\}dY,\end{aligned} \tag{18}$$

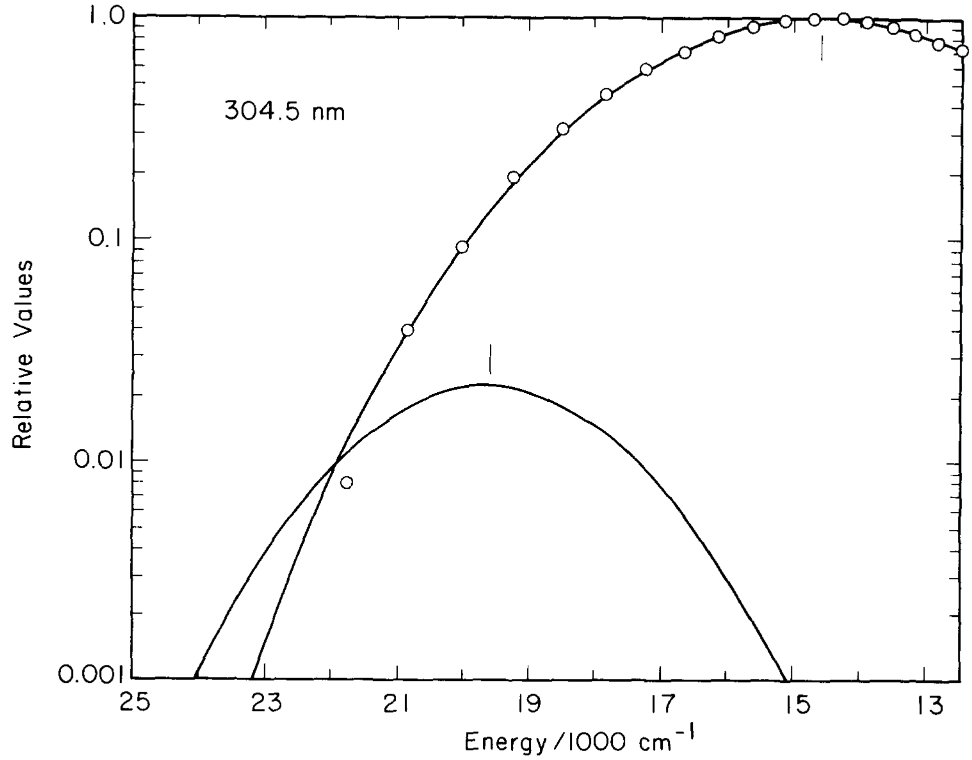

FIG. 11. Same as Fig. 9; photolysis occurred at 304.5 nm.

This article is copyrighted as indicated in the article. Reuse of AIP content is subject to the terms at: http://scitation.aip.org/termsconditions. Downloaded to IP: 128.62.36.173 On: Tue, 25 Nov 2014 22:22:42

TABLE IV. Mean value and standard deviation of the distribution of threshold energies $Y$ in the photolysis of $N_2O_5$, Eq. (15).

| Photolysis wavelength nm | Mean energy $cm^{-1}$ | Standard deviation $cm^{-1}$ |
|---|---|---|
| 266 | 21 000 | 2000 |
| 280 | 20 100 | 2000 |
| 292 | 20 000 | 1900 |
| 304.5 | 19 700 | 1800 |

where $A$ is an indeterminate amplitude factor. The values of $\mu$ and $\sigma$ obtained in fitting the observed $P(X)$ spectrum to Eq. (16) were substituted into Eq. (18), and the upper limit of the integral $E$ was varied from 24 900 to 12 500 in steps of 100 $cm^{-1}$, which gave 125 values of the population POP($E$) for each wavelength of photolysis.

As evaluated by Eq. (18), the relative populations of photolysis produced nitrogen dioxide as a function of energy (internal plus electronic) are given by Fig. 13, where $N_2O_5$ is photolyzed at 266, 280, 292, and 304.5 nm. These populations are red shifted by about 1000 $cm^{-1}$ relative to the distributions of threshold energies, Figs. 8–11. The populations at 266 and 304.5 nm are separated less at low energies than at high energies. The three populations produced at 280, 292, and 304.5 nm show some separation at high energies, but they are almost the same at low energies. One notes an interesting aspect of Fig. 13: the four curves that represent a spread of 4750 $cm^{-1}$ in photolysis energy all approach zero at low energy with no spread for three out of four cases and with the fourth case not far removed. The low energy end of the population appears to be running up against a physical limit. The nature of this physical limit is discussed below.

A partial energy level diagram of $N_2O_5$ and some of its photolysis products are given by Fig. 14. The energies (wave numbers) on the left-hand side of the figure are based on spectroscopic observations and thermochemistry. With the ground state of $N_2O_5$ taken as origin of energy, the energy of ground state $NO_2 + NO_3$ is 7458, ground state $NO_3$ plus $^2B_2$ $NO_2$ is 17 258,[21] ground state $NO_3$ plus $^2B_1$ $NO_2$ is 22 206,[22] and ground state $NO_3 + NO + O$ is 32 573. When $N_2O_5$ is excited by radiation at 266 nm, the energy is 37 594, which is higher than all sets of products on the left of the figure. The maximum of the population of $NO_2^*$ energy (compare Fig. 13) is 19 900 above ground state $NO_2 + NO_3$ or 27 358 $cm^{-1}$ above the origin. At this maximum, the sum of the translational energy of the products and the rovibrational energy of the $NO_3$ fragment is found by difference to be 10 236 $cm^{-1}$.

The fluorescence energy is the sum of the ground state energy of the excited electronic state of $NO_2$ plus the internal energy of the (almost nascent) $NO_2$ photolysis product. The internal energy distribution in the photolysis product $NO_2$ inferred from these experiments depends on what electronic state $NO_2$ is formed in, that is, whether it is $^2B_1$ or $^2B_2$.[19,20] The state $^2B_1$ is linear, and the $^2B_2$ is bent with a more acute angle than the bent ground $^2A_1$ state. There is some uncertainty about the energy origin of these two excited electronic states; the values used in this article are those proposed by Refs. 21 and 22. The most probable value of the internal energy is 10 100 if the $NO_2^*$ state is $^2B_2$, and it is 5152 if the $NO_2^*$ state is $^2B_1$. The inferred population of internal energy falls to zero at about the origin of the $^2B_1$ state, Fig. 14. (The origin of $^2B_1$ is 14 748 $cm^{-1}$, compare Fig. 13.) If the excited molecule is formed in the $^2B_2$ state, then the internal energy of the initially produced $NO_2^*$ is zero from the origin up to almost 5000 $cm^{-1}$, and the population given by the cross-hatched region of Fig. 14 rises above the large energy gap below. The inferred populations from experiments at 280, 292, and 304.5 nm, Fig. 13, all fell to zero at an energy close to the origin of $^2B_1$ state. The crowding together of the low energy population distributions in Fig. 13 suggests that upon photolysis of $N_2O_5$ the $NO_2$ molecule is formed in the

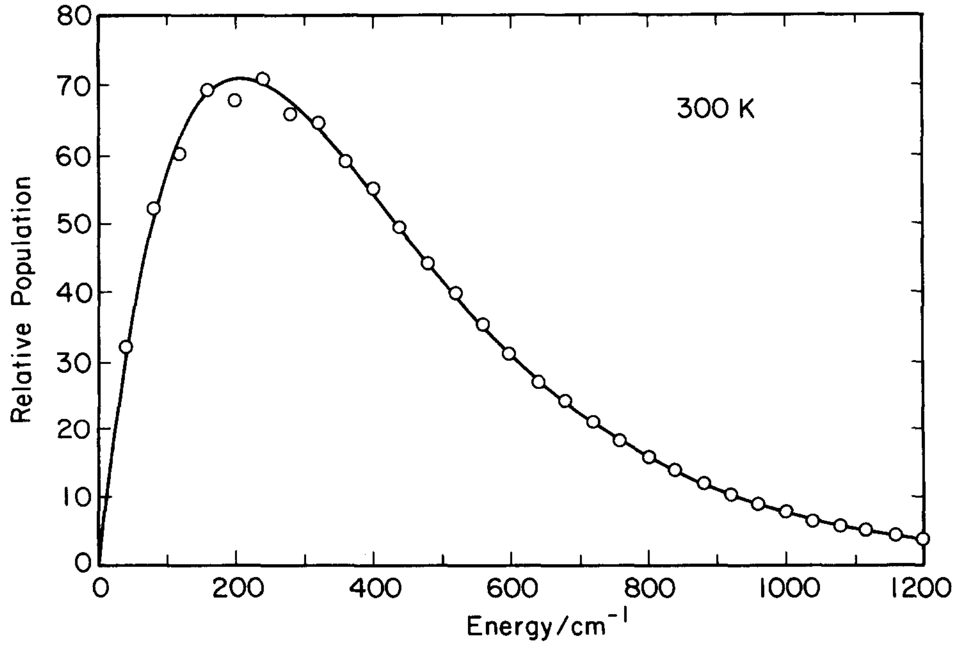

FIG. 12. Rotational–vibrational population of $NO_2$ at 300 K as a function of internal energy: as evaluated by the method of Ref. 18 and using rotational quantum number $K$ from 1 to 12, circles; as approximated by Eq. (17), smooth curve.

This article is copyrighted as indicated in the article. Reuse of AIP content is subject to the terms at: http://scitation.aip.org/termsconditions. Downloaded to IP: 128.62.36.173 On: Tue, 25 Nov 2014 22:22:42

TABLE V. Low-pressure fluorescence lifetimes of $NO_2$ as a function of laser excitation frequency, based on data in Ref. 12. Cases in parentheses were extrapolated beyond the range of observations of Ref. 12. Threshold energies $Y$ are the laser excitation energies plus 600 $cm^{-1}$.

| $\nu/cm^{-1}$ | $\tau/\mu s$ | $\tau/\tau_{REF}$ |
|---|---|---|
| 25 000 | (60.0) | 1.000 |
| 24 000 | (61.0) | 1.017 |
| 23 000 | (62.5) | 1.042 |
| 22 000 | 65.6 | 1.093 |
| 21 000 | 70.4 | 1.173 |
| 20 000 | 80.0 | 1.333 |
| 19 000 | 94.4 | 1.573 |
| 18 000 | 113.6 | 1.893 |
| 17 000 | 137.6 | 2.293 |
| 16 000 | 166.4 | 2.773 |
| 15 000 | 200. | 3.333 |
| 14 000 | (230) | 3.833 |
| 13 000 | (249) | 4.140 |
| 12 500 | (250) | 4.167 |

$^2B_1$ electronic state. Shortly after $NO_2$ is formed, there would be the usual strong interactions between $^2B_1$, $^2B_2$, and $^2A_1$ states, but the nascent internal energy distribution in $NO_2$ is presumably given by Fig. 13 after the origin of the $^2B_1$ state is subtracted off.

There is another line of evidence that indicates $NO_2^*$ is formed in the $^2B_1$ state rather than in the $^2B_2$ state. If it was formed in the $^2B_2$ state, then the translational energy of products plus the internal energy of the four-atomic $NO_3$ radical would be 10 236 $cm^{-1}$ while the internal energy of the triatomic $NO_2$ molecule would average 10 100 $cm^{-1}$, and this situation would imply a strongly nonstatistical partitioning of rovibrational energy between the two products. If $NO_2$ is produced in the $^2B_1$ electronic state, it would have an average internal energy of 5152 $cm^{-1}$ and $NO_3$ could have up to 10 236 $cm^{-1}$ of internal energy, which does not imply a nonstatistical partitioning of internal energy.

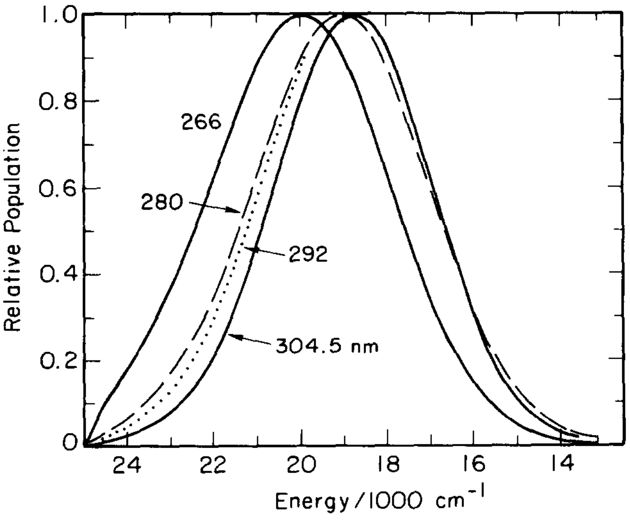

FIG. 13. Relative population of photolysis-produced nitrogen dioxide as a function of internal energy (unresolved rotational, vibrational, and electronic) as deduced from the data using Eq. (18) for photolysis at 266, 280, 292, and 304.5 nm. The complete curve at 292 nm is not shown because it overlaps low energy branch of the curves at 280 and 304.5 nm.

For the case of photolysis of $N_2O_5$ at 304.5 nm, the energy of the electronic state $^2B_1$ (14 748 $cm^{-1}$) was subtracted from the energy distribution, Fig. 13, presumably to give the internal energy distribution relative to zero. The relative population scale is in arbitrary units. At a series of temperatures between 3000 and 4500 K, the equilibrium rotational–vibrational energies of ground-state $NO_2$ were calculated, and the curve at 3500 K was found to have a maximum probability at about the same energy as the internal energy of the PIF curve; this comparison is plotted on Fig. 15. The curves in Fig. 15 are normalized to the same area. The spread of the high temperature equilibrium curve is much larger than that for the nascent $NO_2$ molecules. The internal energy distribution shown in Fig. 15 is not a Boltzmann distribution. The high, narrow distribution of internal energy in the photolysis product can be rationalized to some extent. $^2B_1$ $NO_2$ is linear, and the $NO_2$ group in $N_2O_5$ is bent. The bent structure of the reactant group would contribute a high degree of excited bending vibrational energy to the newly formed $^2B_1$ molecule, which would require a number of collisions to be redistributed into a Boltzmann distribution.

At 266 nm Ravishankara[5] found a 38% yield of atomic oxygen. If atomic oxygen and fluorescence are, respectively, the high and low energy extremes of the same nascent product quantum state, one might expect in Fig. 13 a large finite intercept of the population distribution at the 25 000 $cm^{-1}$ axis, which is close to the threshold for atomic oxygen production. Figure 8 shows a small finite intercept in the distribution of threshold energies on the 25 000 $cm^{-1}$ axis, but the population distribution of Fig. 13 does not show such an intercept. In these experiments the $NO_2$ product molecule has undergone a collision or two during its period of observation, and about 2000 $cm^{-1}$ of energy is removed per collision.[12] Some collisional degradation of the high internal energies of the product molecule is indicated.

Information can be obtained about the quantum yield of $NO_2$ fluorescence from $N_2O_5$ photolysis from the data in Table II and III, which gives relative fluorescence intensities (arbitrary units) per photon absorbed. Table II gives the total undispersed $NO_2$ fluorescence under standard conditions (30 ns delay time, 600 ns observation time) for three wavelengths of excitation and for four pressures of $NO_2$ between 20 and 90 mTorr. The data show substantial scatter, which can be explained. At very high resolution the $NO_2$ absorption spectra between 553 and 648 nm shows over 18 000 peaks rising out of the continuum $NO_2$ spectra.[23] The data in Table III are based on low resolution (1 nm) cross section spectra.[24] Within the range of this low resolution cross section the narrow laser lines used in these experiments could be in some peak or valley of the high resolution spectra, which could cause the scatter in the results of Tables II–III. On this basis the data taken at three different wavelengths are averaged in Table II. The broad features of Tables II–III are: (i) The intensity of the LIF of $NO_2$ decreased by about 35% between pressures of 20 and 90 mTorr, and the intensity of the PIF showed a similar decrease with increasing pressure. (ii) In undispersed ultraviolet PIF experiments (Table III), the intensities induced by radiation at 266, 280, and 292 nm are about the same, but the intensities

This article is copyrighted as indicated in the article. Reuse of AIP content is subject to the terms at: http://scitation.aip.org/termsconditions. Downloaded to IP: 128.62.36.173 On: Tue, 25 Nov 2014 22:22:42

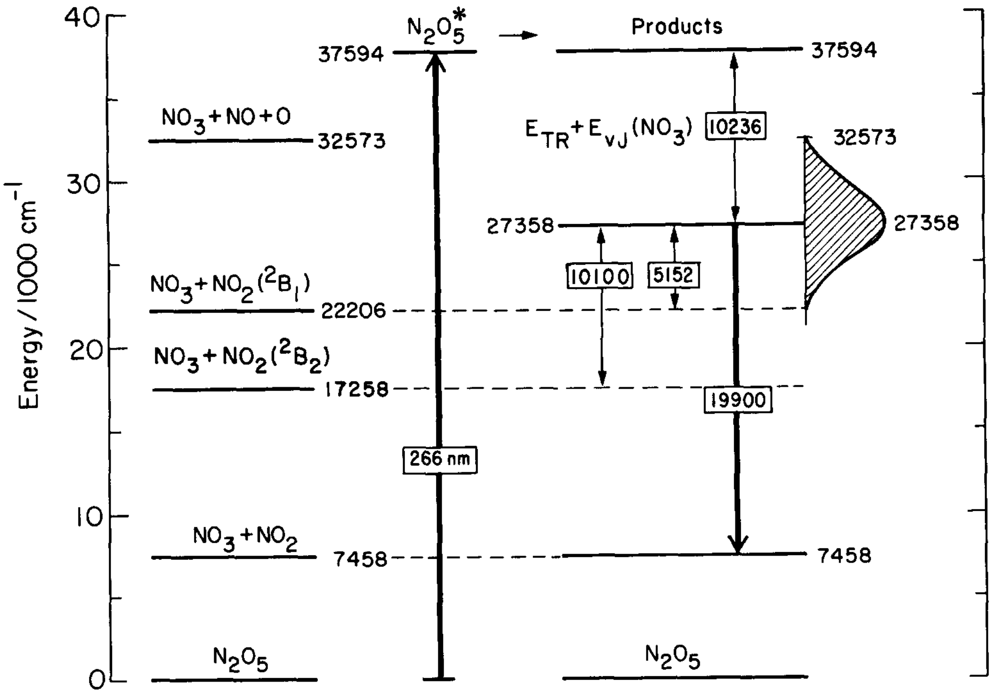

FIG. 14. Energy level diagram for $N_2O_5$ and its photolysis products, when photolysis occurs at 266 nm. As described in the text, the hatched figure gives the inferred internal energy distribution in the (almost) nascent nitrogen dioxide. Notable features of this distribution is that it appears to be cut off at high energies by the energy threshold to produce $NO_3 + NO + O$ and it appears to terminate at the low energy side near the origin of the electronic state $^2B_1$.

upon photolysis at 304.5 and 320 nm are substantially lower, by about a factor of 8. If the average of PIF data at the three shortest wavelengths at 20 to 60 mTorr are compared with the average of the three LIF data over the same pressure range, the quantum yield for PIF is about 0.22 ± 0.1. At the two longest ultraviolet wavelengths the quantum yield for PIF is about 0.03 ± 0.01.

Since the quantum yield of PIF is much less than one, the photolysis of $N_2O_5$ must involve all of the following steps:

$$N_2O_5 + h\nu = NO_3 + NO_2^* = NO_3 + NO + O \qquad (19)$$

$$= NO_3 + NO_2^* = NO_3 + NO_2 + h\nu \qquad (20)$$

$$= NO_3 + NO_2. \qquad (21)$$

The wavelength threshold for Eq. (19) is 307 nm. It is agreed,[2,4,5] that the quantum yield for production of $NO_3$ is about one at all wavelengths. It is interesting to look at the sum of the quantum yields for Eq. (19)[5] plus Eq. (20) from this study:

| Wavelength | Quantum yield | Eq. (19) | Eq. (20) | Sum |
|---|---|---|---|---|
| 248 | | 0.72 | | >0.72 |
| 266 | | 0.38 | 0.25 | 0.63 |
| 289 | | 0.15 | 0.21 | 0.36 |
| 305 | | 0.0 | 0.03 | 0.03 |
| 320 | | | 0.03 | 0.03 |

These results indicate that Eq. (21) occurs in parallel with Eq. (20) at all wavelengths of this study, that is, some $NO_2$ is produced in the $^2A_1$ ground electronic state and some is pro-

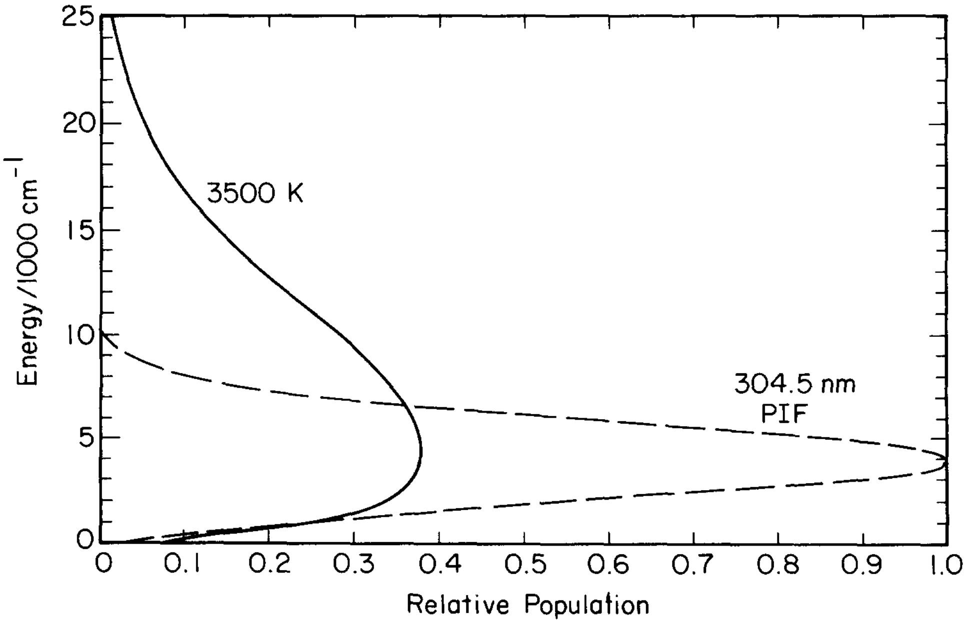

FIG. 15. The internal energy distribution of photolytically produced nitrogen dioxide obtained by subtracting the energy of the electronic state $^2B_1$ from the distribution function including unresolved electronic, rotational, and vibrational energies (Fig. 13) for $N_2O_5$ photolysis at 304.5 nm. This energy distribution is compared with a calculated Boltzmann distribution at 3500 K, which gives a most probable value at about the same energy, and the two curves enclose the same area.

This article is copyrighted as indicated in the article. Reuse of AIP content is subject to the terms at: http://scitation.aip.org/termsconditions. Downloaded to IP: 128.62.36.173 On: Tue, 25 Nov 2014 22:22:42

duced in excited electronic state or states. The sum of the quantum yield for the two processes, Eqs. (19) and (20), that go by way of $NO_2^*$ increases with photolysis energy from the threshold for Eq. (19) up to 248 nm. The sharp decrease of PIF quantum yield between 292 and 304 nm is probably of significance in discussing the mechanism of $N_2O_5$ photolysis, but the reason for it is not apparent.

## CONCLUSIONS

Visible fluorescence from electronically excited $NO_2$ was observed upon the ultraviolet photolysis of $N_2O_5$ at four wavelengths between 266 and 304.5 nm. Two lines of evidence indicate that initially $NO_2$ is produced in the ${}^2B_1$ excited electronic state. By a comparison of the emission spectrum of the photolysis induced fluorescence (PIF) with the laser induced spectra (LIF) of $NO_2$, the internal (undifferentiated rovibrational) energy distribution of the electronically excited product was inferred. This internal energy distribution is highly excited and non-Boltzmann, which may be explained by the large change in geometry of the ${}^2B_1$ state of $NO_2$ and the equilibrium geometry of the $NO_2$ segment of $N_2O_5$.

## ACKNOWLEDGMENTS

This work was supported by the Director, Office of Energy Research, Office of Basic Energy Sciences, Chemical Sciences Division of the U.S. Department of Energy under Contract Number DE-AC03-76SF00098. Laser equipment used in this work was borrowed from the San Francisco Laser Center, supported by the National Science Foundation, NSF Grant No. CHE79-16250 and the National Institute of Health, Grant No. NIH P41 RR01613-02, awarded to the University of California at Berkeley in collaboration with Stanford University.

[1] F. Magnotta, Ph.D. dissertation, University of California, Berkeley, 1979.
[2] D. M. Swanson, B. Kan, and H. S. Johnston, J. Phys. Chem. **88** (1984).
[3] J. J. Margitan, Presented at the XVI Informal Conference on Photochemistry, Harvard University, August 20–24, 1984.
[4] J. R. Barker, L. Brouwer, R. Patrick, M. J. Rossi, P. L. Trevor, and D. M. Golden, Int. J. Chem. Kinet. **17**, 991 (1985).
[5] A. R. Ravishankara, P. H. Wine, C. A. Smith, P. E. Barbone, and A. Torabi, J. Geophys. Res. **91**, 5355 (1986).
[6] B. W. McClelland, L. Hedberg, K. Hedberg, and K. Hagen, J. Am. Chem. Soc. **105**, 3789 (1983).
[7] P. D. Hammer, E. J. Dlugokencky, and C. J. Howard, J. Phys. Chem. **90**, 2491 (1986).
[8] H. H. Nelson, L. Pasternak, and J. R. McDonald, J. Phys. Chem. **88**, 1286 (1983); J. Chem. Phys. **79**, 4279 (1983).
[9] G. Inoue, Y. Nakata, Y. Usui, H. Akimoto, and M. Okuda, J. Chem. Phys. **70**, 3689 (1979).
[10] L. J. Butler, D. Kranovich, Y. T. Lee, O. Ondrey, and R. Berson, J. Chem. Phys. **79**, 1708 (1983).
[11] A. E. Douglas, J. Chem. Phys. **45**, 1007 (1966).
[12] V. M. Donnelly and F. Kaufman, J. Chem. Phys. **66**, 4100 (1977); **69**, 1456 (1978); V. M. Donnelly, D. G. Keil, and F. Kaufman, J. Chem. Phys. **71**, 659 (1979); and references therein.
[13] N. Sugimoto, S. Takezawa, and N. Takeuchi, Jpn. J. Appl. Phys. **21**, 1536 (1982).
[14] P. J. Brucat and R. N. Zare, J. Chem. Phys. **81**, 2562 (1984).
[15] G. Schott and N. Davidson, J. Am. Chem. Soc. **80**, 1841 (1958).
[16] F. Yao, I. Wilson, and H. S. Johnston, J. Phys. Chem. **86**, 3611 (1982).
[17] R. E. Smalley, L. Wharton, and D. H. Levy, J. Chem. Phys. **63**, 4977 (1975).
[18] J. N. Pitts, Jr., J. H. Sharp, and S. I. Chan, J. Chem. Phys. **42**, 3655 (1963).
[19] G. G. Gillespie, A. U. Khan, A. C. Wahl, R. P. Hosteny, and M. Krauss, J. Chem. Phys. **63**, 3425 (1975).
[20] C. F. Jackels and E. R. Davidson, J. Chem. Phys. **65**, 2941 (1976).
[21] (a) A. J. Merer and K. E. J. Hallin, Can. J. Chem. **56**, 838 (1978); (b) J. C. D. Brand, K. J. Cross, and A. R. Hoy, Can. Phys. **57**, 430 (1979); (c) J. L. Hardwick and J. C. D. Brand, Can. J. Phys. **54**, 80 (1976).
[22] J. L. Hardwick and J. C. D. Brand, Chem. Phys. Lett. **21**, 458 (1973).
[23] D. K. Hsu, D. L. Monts, and R. N. Zare, *Spectral Atlas of Nitrogen Dioxide, 5330 to 6480 Å* (Academic, New York, 1978).
[24] R. A. Graham and H. S. Johnston, J. Phys. Chem. **82**, 254 (1978).

This article is copyrighted as indicated in the article. Reuse of AIP content is subject to the terms at: http://scitation.aip.org/termsconditions. Downloaded to IP: 128.62.36.173 On: Tue, 25 Nov 2014 22:22:42